

Magnetization transfer and double-quantum filtered imaging as probes for motional restricted water in tulip bulbs

P. Bendel^{a,*}, H. Zemah^b, R. Kamenetsky^b, F. Vergeldt^c, H. van As^c

^aDepartment of Chemical Services, MR Center, The Weizmann Institute of Science, Rehovot 76100, Israel

^bDepartment of Ornamental Horticulture, ARO, The Volcani Center, Bet Dagan, Israel

^cDepartment of Biomolecular Sciences, Wageningen University, Wageningen NMR Centre, Wageningen, The Netherlands

Received 15 December 2000; accepted 12 May 2001

Abstract

Parameter sensitive MRI experiments were performed on tulip bulbs before and after storage at two different temperatures, 4°C (chilled), and 20°C (non-chilled). Quantitative measurements of the amount of magnetization transfer (MT) in the storage scales of the bulbs, were compared to the average values of the relaxation rates R_1 and R_2 , and the apparent normalized spin density (NSD). At the end of the storage period, bulbs were also scanned using ^1H double quantum (DQ) filtered imaging. Both MT and DQ filtered imaging revealed significant differences between chilled and non-chilled bulbs, which were consistent with the differences observed in the average values of NSD , R_1 , and R_2 . The results indicated a smaller fraction of solid protons (e.g., starch, sugars, and possibly bound water), or less contact between these solid protons and (free) water in the storage scales of the chilled bulbs, after 8 weeks of storage at low temperature. © 2001 Elsevier Science Inc. All rights reserved.

Keywords: Magnetization transfer; Double-quantum filtered imaging; Tulip bulbs; Cold storage; Bound water

1. Introduction

Magnetic Resonance Imaging has been used quite extensively in the investigation of plant systems [1,2]. One of the research objectives in such studies is the characterization of “water status,” distinguishing between “free” and “bound” water. Mobile, or free water, is characterized by relatively long values of T_1 and T_2 , while a shortening of the relaxation times is considered to indicate the presence of bound water, i.e., water associated with macromolecules [3–5]. It is believed that certain metabolic processes in plant systems, such as the release from dormancy in buds of perennial fruit trees [6], or low temperature treatment in tulips bulbs [3], are accompanied by degradation of starch to low molecular-weight sugar molecules. This process could be accompanied by local release of water molecules tightly bound to the starch granules into the bulk water, or by an influx of free water molecules attracted by the higher osmotic potential,

due to the increased sugar concentration, or by a combination of both effects.

The traditional methods to assess and investigate water status in plant systems are the image-based measurements of relaxation rates, R_1 ($1/T_1$), R_2 ($1/T_2$), and the apparent diffusion coefficient (ADC), with the results often calculated and displayed as images of the measured parameters [7]. In this contribution, we report on the application to plant systems of two additional techniques, aimed at assessing the presence and abundance of a solid or motional restricted proton pool: the imaging of the degree of Magnetization Transfer (MT), which is widely used in medical MRI [8], and the imaging of water molecules with some degree of orientational order, using ^1H double quantum filtered (DQF) imaging [9,10]. The rationale for attempting to implement and evaluate these methods in plant systems were based on the notion that they may provide a more direct measure of the bound water pool, independent on model-based fitting procedures which are necessary in the computation and interpretation of R_1 and R_2 images.

MT and DQF MRI were applied to characterize the effect of the storage process on tulip bulbs at different temperatures, in addition to the established techniques of T_1 , T_2 , and

* Corresponding author. Tel.: +972-8-9343186; fax: +972-8-9472218.

E-mail address: peter.bendel@weizmann.ac.il (P. Bendel).

spin density imaging. It is well known that the storage of the bulbs of some geophytes (such as tulips) at low temperature is essential for the successful flowering after planting, yet the reasons for this requirement are poorly understood [11]. In fact, even clear phenomenological differences (structural or functional) between chilled and non-chilled bulbs were not found, except in studies using MRI [3,12,13]. The aims of this study were to determine whether MT and DQF imaging could reliably reveal differences in pre-planting development between chilled and non-chilled tulip bulbs, and whether the results were consistent with those provided by the interpretation of T_1 , T_2 and spin density maps.

2. Magnetization transfer imaging

The classic and simplest experiment to measure MT effects from bound water pools consists of applying a continuous irradiation off-resonance from the free water peak, followed by a readout sequence (which may consist of a single pulse, or an imaging sequence). The signal intensity obtained from such a scan (M_s) is compared to the intensity from a control scan in which the off-resonance irradiation was omitted (M_o). In principle, the influence of the off-resonance irradiation can be divided into two effects, the direct rf effect, and the MT effect. If the irradiation lasts long enough to achieve steady state, and strong enough to fulfill the condition:

$$\omega_l^2 T_1 T_2 \gg 1 \quad (1)$$

where ω_l is the irradiation strength, then the direct rf effect is given by the Bloch equations:

$$\left(\frac{M_s}{M_o}\right)_{rf} = \frac{1}{1 + \frac{T_1}{T_2} \left(\frac{\omega_l}{\Delta\omega_o}\right)^2} \quad (2)$$

where $\Delta\omega_o$ is the frequency difference between the resonance and the irradiation frequencies. The above equation is not restricted to the extreme narrowing limit, but does assume that $T_{1\rho} \approx T_2$, where $T_{1\rho}$ is the relaxation time along the effective field, in the presence of the off-resonance irradiation. If the free water pool is in contact (either by chemical exchange, or by dipolar interactions) with bound water (characterized by a much shorter T_2 than that of the free water), then the irradiation exerts a direct effect on the bound water spins, which can then be transferred to the free water spins. Assuming that a simple first-order exchange process is the dominant mechanism for magnetization transfer, the differential equation describing the longitudinal magnetization of the free water spins is:

$$\frac{dM_{z,f}}{dt} = \frac{M_{o,f} - M_{z,f}}{T_{1,f}} - \frac{M_{z,f}}{\tau_f} + \frac{M_{z,b}}{\tau_b} \quad (3)$$

The subscripts f and b denote the free and bound pools, respectively, and τ is the lifetime of a proton in the respec-

tive pool. $T_{1,f}$ is the relaxation time of the free water in the absence of exchange. Under most practical conditions, the size of the free water pool is much larger than that of the bound water. Therefore, the subscript f will be omitted from the magnetization variables (M_z , M_o , M_s) for the remainder of this paper, for the sake of simplicity.

The magnitude of $M_{z,b}$ is also time dependent, but for steady-state conditions, it can be assumed that $M_{z,b}$ is equal to a constant quantity denoted by ϵ . The steady state also implies that:

$$\frac{dM_z}{dt} = 0 \quad (4)$$

Furthermore, due to the chemical equilibrium:

$$\frac{1}{\tau_f} = \frac{p_b}{\tau_b} \quad (5)$$

where p_b is the fraction of the bound water pool protons. Combining Eqs. [3–5] one arrives that the MT effect is given by:

$$\left(\frac{M_s}{M_o}\right)_{MT} = \frac{\frac{1}{T_{1,f}} + \frac{\epsilon}{\tau_b M_o}}{\frac{1}{T_{1,f}} + \frac{p_b}{\tau_b}} \quad (6)$$

The extent of the MT effect is therefore dependent on the relative size of the bound water pool, p_b , the life time τ_b , and $T_{1,f}$. The larger the fraction p_b , the smaller the signal M_s , and the stronger the MT effect. Moreover, the MT effect is maximal when the bound water magnetization is fully saturated, i.e., when ϵ is minimized (ideally, $\epsilon \approx 0$).

The most important parameter for the practical implementation of MT experiments is the value of $(\omega_l/\Delta\omega_o)$. It should be chosen large enough to minimize ϵ , yet small enough to also minimize the direct rf effect on the free water magnetization (Eq. 2). Fig. 1 shows a simulated curve, plotting the ratio $\left(\frac{M_s}{M_o}\right)_{rf}$ vs. T_1/T_2 , according to Eq. 2. In this simulation, the assumed value for $(\omega_l/\Delta\omega_o)$ was 0.05, which was also the value used in the experiments (see Materials and Methods). According to Fig. 1, this choice of $(\omega_l/\Delta\omega_o)$ appears adequate for minimizing the direct rf effect on the free water signal, since the predicted value of $\left(\frac{M_s}{M_o}\right)_{rf}$ remains close to 1 for situations where the order of the T_1/T_2 ratio is not larger than 10^1 . The expected value of ϵ (i.e., essentially the value of $\left(\frac{M_s}{M_o}\right)_{rf}$ for the bound water spins) is more difficult to predict, since the relaxation rates for the bound spins can usually not be directly measured, and Eq. 2 may not be adequate to accurately describe the direct rf effect of the irradiation on the magnetization of the bound spins. Nevertheless, if one assumes that Eq. 2 still applies approximately for the bound water spins, and that the T_1/T_2 ratio is of the order of 5×10^3 , as was observed

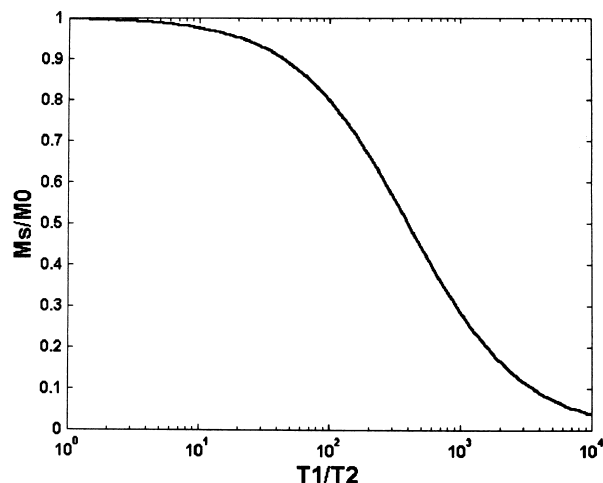


Fig. 1. Calculated curve simulating the direct rf effect as function of T_1/T_2 , for the value $(\omega_r/\Delta\omega_o) = 0.05$.

in muscle tissue [8], then the curve in Fig. 1 predicts that ϵ should be about 0.05, i.e., a close to maximal achievable effect.

3. Double quantum filtered imaging

The application of two time separated rf pulses to coupled $I = 1/2$ spin systems can create multiple quantum coherences, which can then be converted back into observable single quantum coherence by a third pulse. In two-spin systems, zero quantum, and double quantum coherences are possible. Suitable phase cycling can then achieve exclusive detection of the part of the observable signal, which originates from the double quantum coherence [14].

In the case of water molecules, the main source for a signal passing through the double quantum filter phase cycling is the intra-molecular dipolar coupling between the two protons of the water molecule. (Multiple quantum coherences from inter-molecular couplings can be observed at much longer evolution times in the presence of strong field gradients [15,16]).

The pulse sequence used for DQ filtered slice selective MRI is depicted in Fig. 2. It is slightly different from the recently proposed sequences [17], in that the slice selection is performed on the last readout pulse of the DQ filter.

4. Materials and methods

4.1. Plant material

Bulbs of *Tulipa gesneriana* L., cv. Apeldoorn, 10/11 cm in circumference, were obtained from the commercial source in the Netherlands. Fifty mature bulbs were harvested in June 1999, and stored at 20°C for two months. In

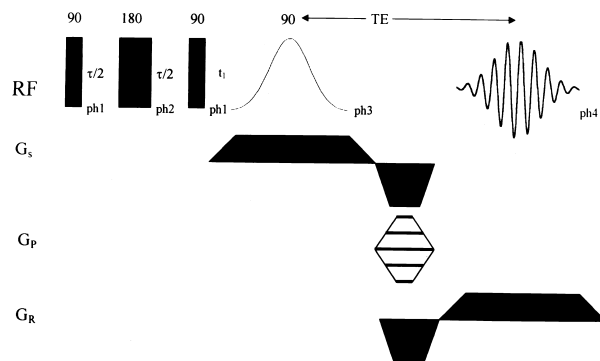


Fig. 2. Pulse sequence used for DQ filtered imaging. The phase cyclings were: $ph1 = 0$; $ph2 = \pi/2, \pi/2, \pi/2, \pi/2, 3\pi/2, 3\pi/2, 3\pi/2, 3\pi/2$; $ph3 = 0, \pi/2, \pi, 3\pi/2$; $ph4 = 0, 3\pi/2, \pi, \pi/2$. For non-selective, DQ filtered spectroscopy, the last gaussian 90° pulse is replaced by a non-selective 90° pulse, followed by signal acquisition.

September, the bulb pool was divided into two equal parts for parallel measurements at the NMR facilities in Rehovot and Wageningen (see below). In September 22, after the first MRI measurements, 25 bulbs were randomly picked and placed at 4°C and 60% relative humidity for four months (chilled bulbs). Twenty five additional bulbs were kept at 20°C and 60–65% relative humidity (non-chilled bulbs). Six intact bulbs per treatment were sampled, tagged and studied by MRI in Israel and the Netherlands. MRI experiments were performed at the beginning of storage treatments and after 8 and 12 weeks of storage.

4.2. NMR experiments

The results were obtained at two separate sites: The scans for the R_1 , R_2 , and spin density images were conducted on a 0.47 T scanner located in the Agricultural University of Wageningen, The Netherlands. This system consists of a 0.47 T electromagnet (Bruker, Karlsruhe, Germany) interfaced to a SMIS spectrometer (Surrey Medical Imaging Systems, Guilford, UK), using a custom-engineered probe containing an rf coil with 50 mm diameter and gradient coils with strengths up to 500 mT/m (Doty Scientific Inc., Columbia, S.C., USA). MT and DQ filtered images were obtained at the Weizmann Institute in Rehovot, Israel, on a 4.7 T superconducting, horizontal bore system (Biospec 47/30, Bruker, Karlsruhe, Germany), using a 7.5 cm diameter 1H resonator supplied by the manufacturer. R_1 and R_2 were also measured at 4.7 T, to verify that appropriate conditions for the MT experiments were met.

R_2 and spin density maps were obtained from a multi-echo sequence described previously [18]. 48 echo images with an inter-echo delay of 4.7 ms were acquired, $TR = 1.5$ s, 128×128 matrix, $FOV = 60$ mm, 2 averages, slice thickness = 3 mm. The parameter images were generated by a pixel-by-pixel fit of the data to a single-exponential decay. R_2 images represent the rate constant of this fitted

decay, and the spin density images the signal extrapolated to $TE = 0$. A small 0.5 mL Eppendorf™ vial containing a 1 mM $MnCl_2$ solution was imaged alongside the bulb, and the spin density values in the bulbs are reported relative to those in the reference tube. R_1 maps were generated from a series of fast spin-echo images, (8 echoes per excitation, effective $TE = 12.2$ ms), and at varying repetition times of $TR = 0.2, 0.35, 0.55, 0.9, 1.5, 2.5,$ and 5 s. $FOV = 60$ mm, 128×128 matrix, 8 averages, slice thickness = 3 mm. The pixel-by-pixel R_1 values were derived by fitting the data to a single-exponential recovery function.

MT images were derived from fast spin echo scans, with and without preceding off-resonance irradiation. A single slice was excited in each scan. Four echoes per excitation were acquired, with effective $TE = 22$ ms, and $TR = 3$ s. $FOV = 5$ cm, 256×256 matrix, slice thickness = 3 mm, 2 averages. A study for each bulb consisted of acquiring irradiation-on and irradiation-off images for two perpendicular planes across the center of the bulb. The off-resonance irradiation was applied during the entire recovery delay in the form of a pulse train with 3.5 ms long pulses interrupted by 0.2 ms long delays. The irradiation strength ($\omega_1/2\pi$) was 510 Hz, and the frequency offset ($\Delta\omega_o/2\pi$) was 10 kHz.

MTC images displaying the quantity $\frac{M_o - M_s}{M_o}$ were calculated on a pixel-by-pixel basis, where M_s and M_o are the image intensities in the presence and absence of the off-resonance irradiation, respectively. It was verified that this protocol caused no measurable MT effect on a phantom containing an aqueous solution of 5 mM $NiCl_2$.

DQ filtered images were acquired with the pulse sequence depicted in Fig. 2, for two bulbs (chilled and non-chilled), after 12 weeks of storage. Slice thickness = 30 mm, $FOV = 8.5$ cm, 64×64 matrix, $TR = 5$ s, $TE = 1.5$ ms, 24 averages. The creation time (τ) was 1 ms. Pulse lengths were 70 μ s for the hard 90° , and 300 μ s for the selective 90° gaussian excitation pulses. The bulbs were placed in the magnet with their longer axis (along the flower bud) oriented in the X-Z plane of the magnetic field, at a $\sim 30^\circ$ angle to the Z axis (the direction of the main magnetic field). Orientation-dependent measurements of the DQ signal were not performed, so that it is possible that stronger effects could have been observed for different orientations.

5. Results

5.1. R_1 , R_2 , and spin density images

Fig. 3 illustrates typical results of calculated spin density images at the beginning and 8 weeks into the storage period. As shown previously, the storage scales exhibit a heterogeneous, layered structure, where wider central regions are separated by narrow border layers [13]. The central regions of the scales are rich in starch granules and serve as the

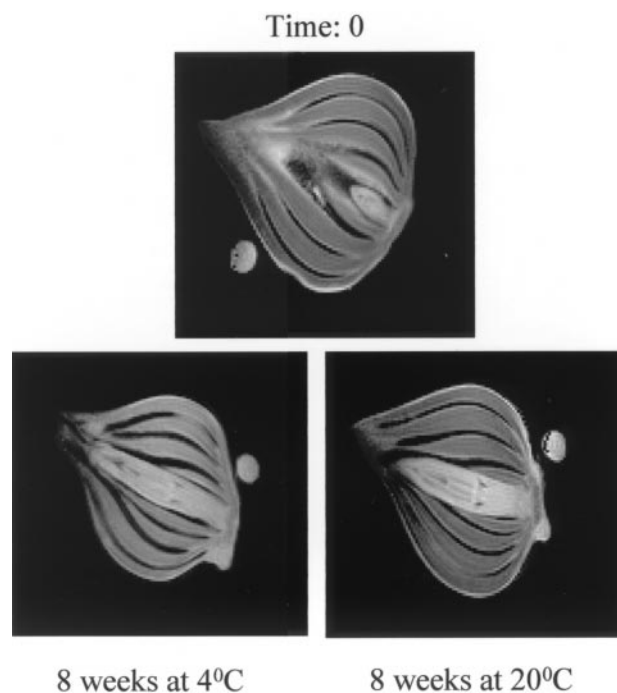


Fig. 3. Cross sections through bulbs displaying the calculated extrapolated spin density, at 0.47 T.

principal storage source for the developing buds. We shall always refer to these regions, when using the description “storage scales” throughout this manuscript. Mean values of the different parameters were calculated by an IDL based image-interactive algorithm, defining regions-of-interest (ROI) which were growing from “seed points” within the storage scales, connecting pixels within a narrowly defined intensity range of typically $\pm 10\%$ around the mean. Typically, about 5×10^3 pixels were included in each ROI. The mean parameter values calculated for each bulb were then averaged over the population in each group (see Materials and Methods). These average values are listed in Table 1.

5.2. MT images

R_1 and R_2 values were determined at 4.7 T for a single bulb, before the beginning of the storage period, to verify that appropriate conditions for the MT experiments were observed. R_1 was measured from a series of snapshot IR gradient echo scans ($TE = 2.2$ ms), with 8 inversion times between 10 ms and 2.5 s. The mean R_1 value in the storage

Table 1
Averaged values of R_1 , R_2 , and normalized spin density (NSD) in the storage scales, at 0.47 T

Bulb population	R_1 (s^{-1})	R_2 (s^{-1})	NSD
Before storage (n = 12)	1.72 ± 0.07	8.5 ± 0.3	0.56 ± 0.03
Storage at $20^\circ C$ (n = 6)	1.77 ± 0.07	10.4 ± 0.7	0.49 ± 0.01
Storage at $4^\circ C$ (n = 6)	1.59 ± 0.03	7.1 ± 0.3	0.61 ± 0.04

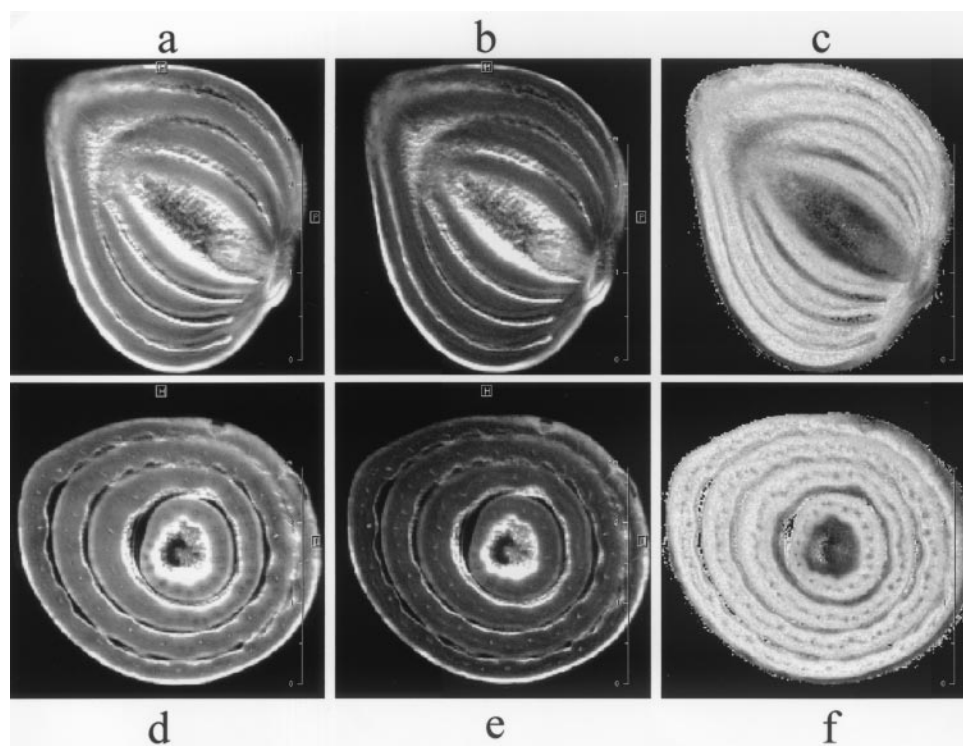


Fig. 4. Cross sections, at two perpendicular orientations through a tulip bulb before the start of the storage period, measured at 4.7 T. Images a and d are without the off-resonance pre-irradiation (M_o), images b and e are following irradiation (M_s), and images c and f are the calculated maps of $MTE = \frac{M_o - M_s}{M_o}$. The calculated values were replaced by 0, if the intensity in images a and d were below a predefined threshold. The gray scales in c and f are mapped linearly between MTE values of 0 and 0.65.

scales was $1.8 \pm 0.15 \text{ s}^{-1}$. The mean R_2 value, determined from single exponential fit to a multi-echo scan with 8 echoes (6 ms – 48 ms) was $34 \pm 4 \text{ s}^{-1}$. Therefore, with a T_1/T_2 ratio of about 19, using the irradiation condition of $(\omega_1/\Delta\omega_o) = 0.05$ should only cause a minimal direct rf effect (see Fig. 1).

Fig. 4 displays results from a bulb scanned before the onset of the storage period. Images displaying the quantity $\frac{M_o - M_s}{M_o}$ were analyzed as described in the previous section, using the scanner's standard image processing software, with ROI's typically containing about 1.5×10^4 pixels. Mean values for each bulb were calculated from both slices. Fig. 5 shows the calculated MT images for two bulbs (chilled and nonchilled) after 8 weeks of storage. The averaged values of the measured MT effect are listed in Table 2. The results obtained from the two perpendicular slices were treated as independent measurements for the calculation of average and standard deviation.

5.3. DQ filtered spectroscopy and imaging

In homogeneously ordered systems, such as tendons, the DQ filtered signals exhibit very characteristic splittings which can help in distinguishing those signals from residual single quantum (SQ) signals which passed the DQ filter due

to experimental imperfections. This is particularly true for ^2H NMR, but also to some extent, for proton signals. However, in general, ^1H DQ filtered signals may represent a distribution of different orientations, residual coupling constants, and exchange rates [19], all contributing to a broad signal of ill-defined shape. This situation was encountered in the tulip bulbs, and therefore particular care was taken to assure that the detected signals are genuine DQ filtered signals. One of the means for verification was the use of a phase-cycling scheme proposed in ref. [9], whereby the phases of the pulses in the creation sequence (ph1 and ph2 in Fig. 2) are incremented by $\pi/2$ and the signals added to those with the regular phase cycling. This creates a π phase shift for the DQ signals, thereby causing their elimination, while the magnitude of residual parasitic SQ signals should not be affected. The scheme is denoted as "DQ-zero" phase cycling. Fig. 6 displays two DQ filtered spectra from a tulip bulb (after 12 weeks storage at 20°C) with regular phase cycling, and with the DQ-zero phase cycling, demonstrating that the suppression of residual SQ signal is adequate.

Another characteristic feature of the DQ-filtered signal is its dependence on the creation time τ . Fig. 7 shows the signal intensity vs. creation time for a chilled and nonchilled tulip bulb. The signal intensities are relative to the total SQ water signal from each bulb. According to this experiment, the total DQ filtered signal in the bulb stored at

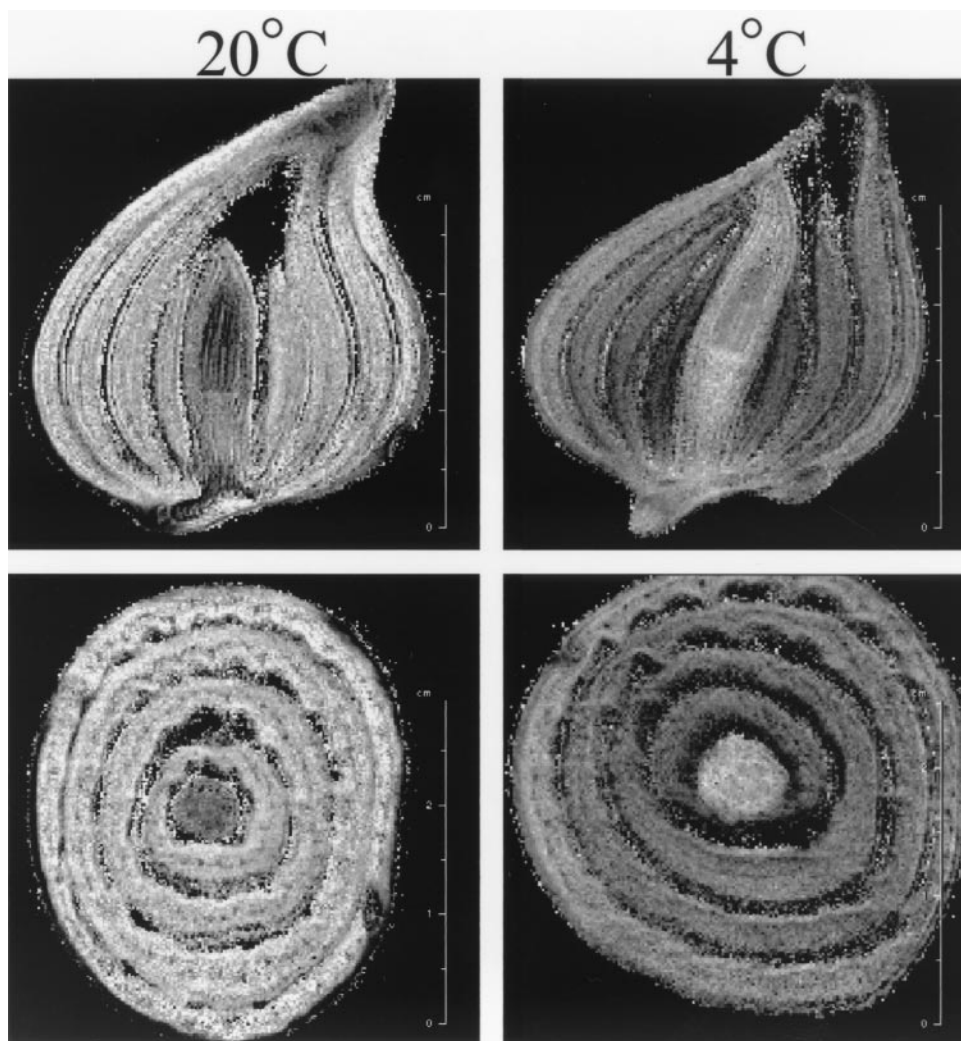


Fig. 5. MTE images at 4.7 T from tulip bulbs after 8 weeks storage at 20°C and 4°C. The gray scales are linearly mapped between 0.2 and 0.6.

20°C is about twice as high as in the chilled bulb. A similar result was obtained in a DQ filtered imaging experiment, where the same two bulbs were imaged side by side (Fig. 8). The integrated intensity measured over the entire bulbs cross sections is 1.45 times higher in the image of the bulb stored at 20°C. A similar image acquired with “DQ-zero” phase cycling showed much weaker and about equal intensities for both bulbs.

Table 2

Averaged values of $MTE = \frac{M_0 - M_s}{M_0}$ in the storage scales, measured at 4.7 T

Bulb population ^a	MTE
Before storage (n = 20)	0.553 ± 0.029
Stored at 20°C (n = 10)	0.507 ± 0.016
Stored at 4°C (n = 10)	0.371 ± 0.036

^a Axial and coronal slices were considered independent measurements for the statistics. The number of bulbs was n/2.

6. Discussion

NMR offers a unique opportunity for non-invasive characterization of developmental metabolic processes in plant systems. Ideally, metabolites could be directly detected using various forms of spatially localized MRS [20–22]. However, ¹H MRI of water is still the most straightforward, accessible and sensitive NMR probe for biologic tissue. Unfortunately, changes in various parameters measurable with ¹H MRI may only be indirect reporters of the actual physical processes, and often, different biophysical interpretations are consistent with the same observed results. Water NMR relaxation times in biologic tissue are usually interpreted in terms of partition of the water molecules between at least two types of environment: a free state, where the water molecules experience similar motional (rotational and translational) freedom as in bulk water, and a restricted, or bound state, where this motional freedom is inhibited, usually by association with macromolecules. The bound water molecules are usually not detectable in con-

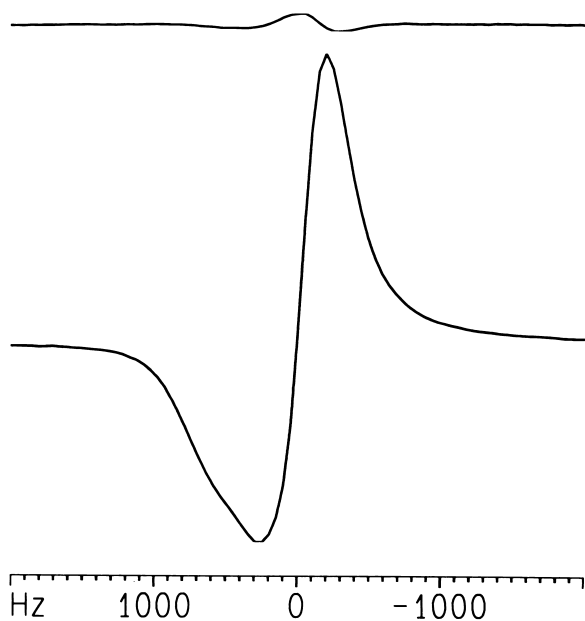


Fig. 6. ^1H spectra at 4.7 T from a bulb stored at 20°C for 12 weeks. The lower trace was acquired with DQ filter phase cycling, and the upper trace with “DQ-zero” phase cycling. No. of scans = 32, repetition time = 5 s, $\tau = 1$ ms.

ventional MRI experiments, due to their short T_2 values, but the bound/free water partition may be inferred, under the right circumstances, from the relaxation rates of the observable free water. Definitive quantitative interpretations are difficult, due to their dependence on many variables, such as exchange and cross relaxation rates [23–25]. In plant tissue, this picture is further complicated by the sub-cellular compartments such as the vacuole, the cytoplasm, the cell wall, and the exchange rates between these compartments. The results of relaxation rate measurements could be affected by many factors besides bound/free water balance, such as

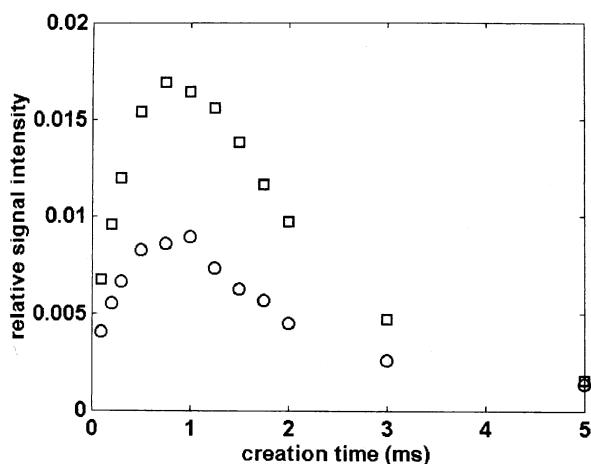


Fig. 7. Intensity of the DQ filtered spectroscopic signal, measured at 4.7 T, from a chilled (circles) and non-chilled bulb (squares), after 12 weeks storage, vs. the creation time τ .

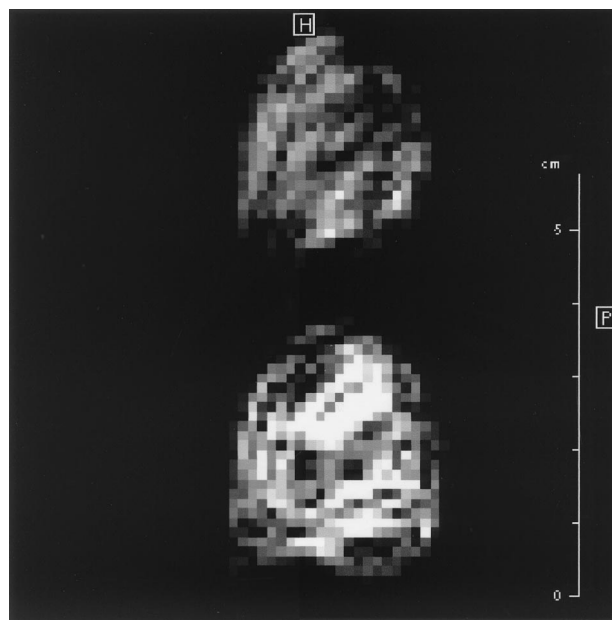


Fig. 8. DQ filtered images at 4.7 T, of a cross section through a chilled (upper) and non-chilled (lower) bulb, after 12 weeks storage.

changes in the size of vacuoles, tonoplast permeability, and (for transverse relaxation) local susceptibility gradients [18, 26,27]. For a unique explanation of results, a combination of the different NMR parameters and anatomic information is needed [28–30].

In this contribution, we explored the feasibility and usefulness of MT and DQ filtered MRI as additional tools for assessing the local partition between bound water and free water in plant systems. In using the bound water concept, we have to realize that the MT effect originates from all protons with short T_2 values (shorter than $\sim 100 \mu\text{s}$ for an offset of 10 kHz) which are in contact (exchange) with the free water fraction. The bound water fraction may include protons of the solid matrix, e.g., cellulose chains, starch, and other saccharides. In scales of tulip bulbs, a large amount of amyloplasts (starch granules surrounded by membranes [13]) are present. During the storage period, the starch in these granules degrades and is (partly) converted to sugars [13,31]. The extent of the MT effect depends upon the fraction of bound water, or the exchange/contact between this proton fraction and the free water pool, and can be measured in a deterministic manner from MRI results, without the need for model-dependent parameter fitting. DQ filtered imaging is unique (compared to the other methods) in that it measures a motional restricted water population directly, rather than through its influence on the free water signal. One should be careful, however, to emphasize that the DQ filtered signal represents water molecules restricted in the orientation rather than the rate of their motion. Therefore, the population of water molecules giving rise to the DQ filtered signal, may not overlap at all with the bound water or solid protons population inferred from the relaxation and MT measurements.

Mapping of the MT effect (MTE) in the storage scales of tulip bulbs after 8 weeks of storage, revealed clear differences between bulbs which were stored at 20°C and 4°C. The MTE in the chilled bulbs was significantly lower, indicating a smaller fraction of solid protons, which could be either in the form of bound water molecules, or starch protons, or both. In this particular comparison, the results of the conventional MRI methods (R_1 , R_2 , spin density) were consistent with the MTE results. The slower R_1 and R_2 and the higher spin density in the chilled bulbs can be interpreted as indicating a smaller fraction of bound (or a larger fraction of free) water. However, when considering the development of the non-chilled bulbs during the storage period, this picture does not hold. The decrease in spin density and the faster R_1 and R_2 after 8 weeks of storage (compared to 0 weeks) may indicate a larger fraction of bound water, but the MTE also slightly decreased, apparently indicating the opposite.

The DQ filtered signal in a chilled bulb was significantly lower than that of a bulb stored at 20°C, indicating a smaller amount of orientational restricted water molecules after storage at 4°C. All the above results are consistent with the hypothesis that cold storage of tulip bulbs enhances or facilitates metabolic processes in the storage scales, which are accompanied by conversion of bound (and/or partially ordered) water to free water. The results also indicate that local water status may be affected not only by local metabolism, but also by migration of free water between different organs in the bulb, as suggested previously [13], driven by local metabolism and accompanied by changes in contact between the solid protons and (free) water in the storage scales.

In summary, it was demonstrated that MT contrast imaging adds to the understanding of water status in tulip bulbs, and presumably also in other plant systems. Since RF irradiation exposure is not a limiting factor, as in medical MRI, continuous strong off-resonance irradiation can be used for good saturation of the restricted water pool. The results of DQ filtered imaging are preliminary, indicating that there are water molecule populations giving rise to such a signal in plant systems, although in tulip bulbs the size of this population is relatively much smaller than in well ordered systems such as tendon. Consequently, the spatial resolution of such images in the systems that we investigated was rather poor. It is possible that DQ filtered imaging could be an interesting approach in other plant systems with clear orientational anisotropy, such as stems or organs containing fibers.

Acknowledgments

This research was supported by the EU-TMR program (contract ERBFMGECT950066) for access to the large scale NMR facility in Wageningen, and by the Foundation of the Chief Scientist of the Ministry of Agriculture in Israel.

We are grateful to the Tel-Aviv University research group (G. Navon, U. Eliav, H. Shinnar, L. Tsoref) for helpful tips on DQF imaging.

References

- [1] Chudek JA, Hunter G. Magnetic resonance imaging of plants. *Progr in Nucl Magn Reson Spectr* 1997; 31:43–63.
- [2] Faust M, Wang PC, Maas M. The use of magnetic resonance imaging in plant science. In: Janick J, editor. *Horticultural Reviews*. Vol. 20. John Wiley & Sons, Inc., 1997. p. 225–65.
- [3] Iwaya-Inoue M, Okubo H, Matsuo E, Motooka K, Ishida N, Koizumi M, Kano H. Characterizing chilling responses for tulip bulbs by ^1H -NMR imaging in relation to metabolic activity. *Cryo-Lett* 1996; 17:241–8.
- [4] Erez A, Faust M, Line MJ. Changes in water status in peach buds on induction, development and release from dormancy. *Sci Hortic* 1998; 73:111–23.
- [5] Parmentier CM, Rowland LJ, Line MJ. Water status in relation to maintenance and release from dormancy in blueberry flower buds. *J Amer Soc Hort Sci* 1998; 123:762–9.
- [6] Faust M, Erez A, Rowland LJ, Wang SY, Normann HA. Bud dormancy in perennial fruit trees: physiological basis for dormancy induction, maintenance, and release. *HortScience* 1997; 34:623–9.
- [7] Clark CJ, Richardson AC, Marsh KB. Quantitative magnetic resonance imaging of Satsuma mandarin fruit during growth. *HortScience* 1999; 34:1071–5.
- [8] Wolff SD, Balaban RS. Magnetization transfer contrast (MTC) and tissue water proton relaxation *in vivo*. *Magn Reson Med* 1989; 10: 135–44.
- [9] Tsoref L, Shinar H, Navon G. Observation of a ^1H double quantum filtered signal of water in biological tissues. *Magn Reson Med* 1998; 39:11–17.
- [10] Seo Y, Ikoma K, Takamiya H, Kusaka Y, Tsoref L, Eliav U, Shinar H, Navon G. ^1H double-quantum-filtered MR imaging as a new tool for assessment of healing of the ruptured Achilles tendon. *Magn Reson Med* 1999; 42:884–9.
- [11] DeHertogh AA, Le Nard M. Physiological and biochemical aspects of flower bulbs. In: De Hertogh AA, LeNard M, eds. *The Physiology of Flower Bulbs*. Elsevier, Amsterdam, 1993. p. 53–69.
- [12] Zemah H, Bendel P, Rabinowitch HD, Kamenetsky R. Visualization of morphological structure and water status during storage of *Allium aflatunense* bulbs by NMR imaging. *Plant Science* 1999; 147:65–73.
- [13] Van der Toorn A, Zemah H, Van As H, Bendel P, Kamenetsky R. Developmental changes and water status in tulip bulbs during storage: Visualization by NMR imaging. *J Exp Bot* 2000; 51:1277–87.
- [14] Bax A, Freeman R, Kempell SP. Natural abundance ^{13}C - ^{13}C coupling observed via double-quantum coherence. *J Am Chem Soc* 1980; 102:4849–51.
- [15] Rizi RR, Ahn S, Alsop DC, Garrett-Roe S, Mescher M, Richter W, Schnall MD, Leigh JS, Warren WS. Intermolecular zero-quantum coherence imaging of the human brain. *Magn Reson Med* 2000; 43:627–32.
- [16] Zhong J, Chen Z, Kwok E. *In vivo* intermolecular double-quantum imaging on a clinical 1.5 T MR scanner. *Magn Reson Med* 2000; 43:335–41.
- [17] Tsoref L, Eliav U, Seo Y, Shinar H, Navon G. Slice-selective proton double quantum filtered MRI of joint connective tissues. *J Magn Reson Imag* 2000; 11:336–41.
- [18] Edzes HT, Van Dusschoten D, Van As H. Quantitative T_2 imaging of plant tissues by means of multi-echo MRI microscopy. *Magn Reson Imag* 1998; 16:185–96.
- [19] Eliav U, Navon GA study of dipolar interactions, and dynamic processes of water molecules in tendon by ^1H , and ^2H homonuclear, and

- heteronuclear multiple quantum filtered NMR spectroscopy. *J Magn Reson* 1999; 137:295–310.
- [20] Ishida N, Ogawa H, Koizumi M, Kano H. Ontogenetic changes of the water status and accumulated soluble compounds in growing cherry fruits studied by NMR imaging. *Magn Reson Chem* 1997; 35:S22–S28.
- [21] Heidenreich M, Kockenberger W, Kimmich R, Chandrakumar N, Bowtell R. Investigation of carbohydrate metabolism and transport in castor bean seedlings by cyclic J cross polarization imaging. *J Magn Reson* 1998; 132:109–24.
- [22] Metzler A, Kockenberger W, Vonkienlien M, Komor E, Haase A. Quantitative measurement of sucrose distribution in ricinus-communis seedlings by chemical shift microscopy. *J Magn Reson Ser B* 1994; 105:249–52.
- [23] Zimmermann JR, Brittin WE. Nuclear Magnetic Resonance studies in multiple phase systems: lifetime of a water molecule in an adsorbing phase on silica gel. *J Phys Chem* 1957; 61:1328–33.
- [24] Foster KR, Resing HA, Garroway AN. Bounds on “bound water”: Transverse nuclear magnetic resonance relaxation in barnacle muscle. *Science* 1976; 194:324–6.
- [25] Edzes HT, Samulski ET. The measurement of cross-relaxation effects in the proton NMR spin-lattice relaxation of water in biological systems: Hydrated collagen and muscle. *J Magn Reson* 1978; 31: 207–29.
- [26] Donker HCW, Van As H, Edzes HT, Jans AWH. NMR imaging of white button mushroom (*agaricus bisporis*) at various magnetic fields. *Magn Reson Imag* 1996; 14:1205–15.
- [27] Donker HCW, Van As H, Snijder HJ, Edzes HT. Quantitative ¹H-NMR imaging of water in white button mushrooms (*agaricus bisporis*). *Magn Reson Imag* 1997; 15:113–21.
- [28] Donker HCW, Van As H. Cell water balance of white button mushroom (*Agaricus bisporus*) during its post-harvest lifetime studied by quantitative magnetic resonance imaging. *Biochim Biophys Acta* 1999; 1427:287–97.
- [29] Van der Weerd L, Ruttnik R, van Dusschoten D, Vergeldt FJ, de Jager PA, Van As H. Plant growth studies using low field NMR. In: Blumler P, Blumich B, Botto R, Fukushima E, editors. Spatially resolved magnetic resonance. Weinheim: Wiley-VCH, 1998. p. 473–9.
- [30] Callaghan PT, Clark CJ, Forde LC. Use of static and dynamic NMR microscopy to investigate the origins of contrast in images of biological tissues. *Biophys Chem* 1994; 50:225–35.
- [31] Lambrechts H, Rook F, Kollofel C. Carbohydrate status of tulip bulbs during cold-induced flower stalk elongation and flowering. *Plant Physiol* 1994; 104:515–20.